Rev.Adv.Mater.Sci. 15(2007) 24-32

REACTIVITY OF $Cr(CO)_6$ IN ATMOSPHERIC PRESSURE CVD PROCESSES FOR THE GROWTH OF VARIOUS METALLURGICAL COATINGS

A. Douard[1], F. Maury[1], J. B. Jorcin[1], N. Pebere[1], J. P. Bonino[1] and H. Glenat[2]

[1]CIRIMAT, UMR5085 CNRS-INPT-UPS, ENSIACET, 118 Route de Narbonne, Toulouse 31077, France
[2]PROMES, Technosud, Rambla de la Thermodynamique, Perpignan 66100, France

Received: January 22, 2007

Abstract. Metalorganic precursors allow a significant decrease of the deposition temperature in CVD processes. When they are employed under atmospheric pressure and using direct liquid injection delivery systems, new processes can be developed for the growth of metallurgical coatings. However, even for a single precursor the great variety of reactive gas phase leads to various coatings with different properties. Original nanocrystalline CrC_xO_y and CrN_xO_y films were deposited in a laminar flow reactor by MOCVD and DLICVD using $Cr(CO)_6$ as molecular precursor in the temperature range 285-450 °C. Pyrolysis was carried out in different ambient including N_2, H_2, NH_3, THF, and toluene. The influence of the various atmosphere on the composition, structure and, consequently, mechanical properties and corrosion behavior of these coatings is discussed.

1. INTRODUCTION

Most of the protective metallurgical coatings are deposited using batch processes which frequently require either high vacuum systems like PVD techniques, or the use of toxic baths for which alternative processes have to be found to respect the new environmental rules. The continuous deposition is technically possible under very low pressure but it requires heavy technology equipment, high investment and high energy costs. Atmospheric pressure CVD is an attractive process for on-line strip coatings on metal pieces if two key points are overcome: *(i)* a sufficiently low deposition temperature and *(ii)* a high growth rate. It is well known that the use of metalorganic compounds as molecular precursors significantly decreases the deposition temperature, which satisfies the first requirement. However, metalorganic precursors have two major drawbacks for industrial applications. First, they generally exhibit poor thermal stability, which permits deposition at low temperature but, as a result, the heating in conventional vaporization bubbler (or saturator) for a long period needed to increase their vapor flow rate and consequently the growth rate leads to premature decomposition prior to the deposition zone. Secondly, many of the metalorganic precursors are solid compounds and when the carrier gas passes through the powder to deliver the precursor vapor an agglomeration is frequently observed and, furthermore, it is also well known that the exchange surface for mass transfer between the carrier gas and the powder decreases as the precursor is consumed and both phenomena make a stable and accurate control of the precursor flow rate difficult. To overcome this problem, several solutions have been proposed based

Corresponding author: F. Maury, e-mail: francis.maury@ensiacet.fr

on flash vaporization of (*i*) a precursor powder [1], (*ii*) an aerosol produced by ultrasonic technique (AACVD or Pyrosol) [2], (*iii*) the spray of a pulsed direct liquid injection of the precursor solution (DLICVD) [3,4]. These delivering systems can meet the second requirement above mentioned.

Combination of atmospheric pressure, MOCVD and DLI system is a route for new metallurgical coatings and, possibly, for continuous deposition processes. However, even for a single source precursor there is a great variety of gas phase mixtures whose reactivity must be investigated resulting from the addition of various reactive gases or from the presence of the solvent as in DLICVD. The prediction of the deposited phase is very hard because of the complexity of the reactive gas phase and of the low temperature that favors a kinetic control of the process, which frequently leads to the growth of metastable phases [5].

DLICVD was essentially used for the growth of simple [4] and complex [6] oxide layers, noble metal films like Ir [7] or Ag [8] and also (Al,Ti)N diffusion barrier [9]. It is noteworthy that most of the DLICVD processes were developed for microelectronic applications and they generally operated under low pressure. There is no report to our knowledge on DLICVD of non oxide coatings for metallurgical applications and this work addresses this goal.

We have a long standing interest in MOCVD under low pressure in the Cr-C-N system [5,10,11], specially using $Cr(CO)_6$ as precursor [12-14]. Recently, we have also investigated the DLICVD using $Cr(CO)_6$ [14]. In this paper, we report the main properties of Cr-based coatings grown by CVD under atmospheric pressure using $Cr(CO)_6$ as precursor under different ambient including various gases added in MOCVD and the solvents used in DLICVD. The reactivity of this precursor is discussed. Chromium oxycarbides and chromium oxynitrides coatings were deposited using the same laminar flow CVD reactor and the different processes are compared. The results are discussed in relation with previous data reported for CrC_xO_y coatings grown by low pressure MOCVD [15-18] and PVD [19]. For chromium oxynitrides, we only found works on PVD [20] for comparison with our results.

2. EXPERIMENTAL

The coatings were deposited in a vertical cold wall CVD reactor. 304L-type stainless steel plates (1x1x0.05 cm^3) and Si(100) wafer (1x1 cm^2) were used as substrates after cleaning as previously reported [13]. They were placed on a SiC-passivated graphite susceptor heated by HF induction. After 24 h under vacuum, the reactor was pressurized with nitrogen to 10^5 Pa. The gas streams (N_2, H_2, and NH_3) were monitored using mass flow controllers with a total flow rate fixed at 5000 sccm to get a constant laminar flow.

For the MOCVD processes, $Cr(CO)_6$ powder was placed in a thermostated saturator (60 °C) in order to control its vapor pressure and subsequently the flow rate. N_2 was used as carrier gas. For the DLICVD processes, saturated solutions of $Cr(CO)_6$ in THF (0.070 M) and toluene (0.022 M) were used. The liquid solution was maintained at room temperature in a pressurized vessel under $3 \cdot 10^5$ Pa of N_2. It was injected in the evaporator under atmospheric pressure. The amount of injected solution increases with the injection frequency, the injector opening time, the differential pressure between the pressurized vessel and the vaporization chamber, and it depends also on the viscosity of the precursor solution. The evaporator was co-axially linked to the vertical CVD reactor. Flash vaporization was achieved at 250 °C and the vapor of solvent and precursor was transported using N_2 from the injector nozzle to the substrates. Under atmospheric pressure, an efficient flash evaporation requires opening times (<0.5 ms) shorter than those used in low pressure DLICVD and this limits the precursor flow rate. For all processes, when a reactive gas was used (H_2, NH_3) it was added at the entrance of the reactor.

The structure of the coatings was determined by X-ray diffraction (Cu Kα). The chemical composition was analyzed by electron probe microanalysis (EPMA) and the surface morphology was examined by scanning electron microscopy (SEM). Adhesion of the coatings on stainless steel substrates was characterized using a scratch tester (Revetest, CSM Instrument) with a Rockwell indenter (R=200 μm). The coatings were scratched under a normal loading rate of 10 N/min and a scratching rate of 1.29 mm/min. The hardness and elastic modulus were determined using a NanoIndenter™ II using indentation loads in the range 0.5-2.5 mN [21].

3. RESULTS AND DISCUSSION

3.1. Growth kinetics

Chromium oxycarbides and chromium oxynitrides coatings were deposited using the conditions reported in Table 1. Deposition in the MOCVD pro-

Table 1. Growth conditions of the various CVD processes using $Cr(CO)_6$ as chromium molecular precursor. All runs were performed in the same vertical cold wall reactor using similar hydrodynamic conditions (atmospheric pressure, total gas flow rate 5000 sccm).

Process	Reactive gas mixture	Coating type	Deposition Temperature (°C)	$Cr(CO)_6$ mole fraction (ppm)	X_R/X_P [a]
MOCVD #1	$Cr(CO)_6/N_2$	fcc CrCO	285	100-338	0
MOCVD #2	$Cr(CO)_6/N_2/H_2$	amorph CrO	285	30-49	1230-2010
MOCVD #3	$Cr(CO)_6/N_2/NH_3$	fcc CrNO	285-300	28-274	125-2170
DLICVD #4	$Cr(CO)_6/N_2$/THF	fcc CrCO	350	98-649	0
DLICVD #5	$Cr(CO)_6/N_2$/Toluene	fcc CrCO	350-450	47-226	0
DLICVD #6	$Cr(CO)_6/N_2$/Toluene/NH_3	fcc CrNOC	350-400	50	1150-1190

a) mole fraction ratio between H_2 or NH_3 and $Cr(CO)_6$.

Table 2. Typical features and properties of representative coatings grown on stainless steel by MOCVD and DLICVD under atmospheric pressure using $Cr(CO)_6$ as precursor (the thickness was approximately 900 nm).

Features/Properties[a]	Chromium oxicarbide		Chromium oxinitride	
Process[b]	MOCVD #1	DLICVD # 5	MOCVD # 3	DLICVD # 6
Structure	fcc CrC_xO_y	fcc CrC_xO_y (nanocryst.)	fcc CrN (285 °C) fcc CrN_xO_y (300 °C)	fcc $CrN_xO_yC_z$ (nanocryst.)
Composition	$Cr_{0.58}C_{0.16}O_{0.26}$	$Cr_{0.48}C_{0.05}O_{0.47}$ (350 °C) $Cr_{0.57}C_{0.25}O_{0.19}$ (450 °C)	$Cr_{0.48}N_{0.43}O_{0.06}C_{0.03}$ (285 °C) $Cr_{0.43}N_{0.20}O_{0.32}C_{0.05}$ (300 °C)	$Cr_{0.24}N_{0.26}O_{0.36}C_{0.13}$
Morphology	+ Very porous, cauliflower-like	+++ Compact (350 °C) very compact (450 °C)	++ Very compact Fine-grained	++ Very compact
Thermal stability[c]	$Cr_2O_3 + Cr_3C_2$ at 650 °C	nd	> 650 °C	nd
Adhesion:	+	++	+++	nd
L_{down} (N)	4-7	5	20	
L_{up} (N)	22-35	18-25	35	
Hardness (GPa)	nd	16	= 6	= 6
Corrosion[d]	+	nd	+++	++

a) + poor, ++ good, +++ very good; nd = not determined.
b) The growth conditions are given in Table 1.
c) After annealing under vacuum for 5 h.
d) In aerated NaCl 0.5M solution.

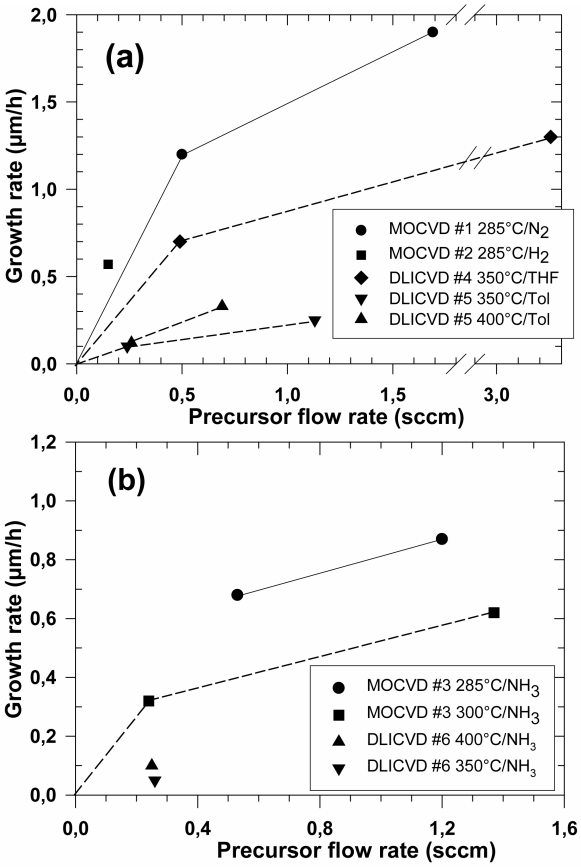

Fig. 1. Influence of $Cr(CO)_6$ flow rate on the growth rate in the various CVD processes (the lines are just a guide for the eyes).

cesses occurs at low temperature (285 °C) while the presence of solvent vapor in DLICVD requires significantly higher temperatures (≥350 °C). This temperature increase could be necessary to compensate the endothermicity of the flash vaporization of the solvent and also because the solvent molecules change the decomposition mechanisms of $Cr(CO)_6$ and are involved in surface reactions. For all processes the growth rate increases with the precursor flow rate and the substrate temperature (Fig. 1). In MOCVD, H_2 was found to show no influence on the growth rate while in DLICVD using a comparable precursor flow rate the growth rate depends on the solvent and is generally lower than in MOCVD processes, even at higher temperatures. Similar behaviors are observed in presence of NH_3. At this stage, no attempt was made to optimize the growth rate by DLICVD.

3.2. Morphology and structure

CrC_xO_y coatings grown under N_2, H_2, and THF atmosphere exhibit a rough, columnar and porous morphology made up of nodular and cauliflower-like grains (Fig. 2). They have a dull gray appearance, except those grown under H_2 that are darker. This porous morphology is not favorable for protective coating applications. The CrC_xO_y films deposited by DLICVD using toluene as solvent exhibit a mirror like appearance with a very smooth surface morphology and a high compactness. In DLICVD, the influence of the solvent is clearly seen by comparing coatings grown using THF and toluene under the same conditions (Fig. 2). Except for the coatings grown under H_2 that are amorphous (process #2), as-deposited chromium oxycarbide films exhibit a nanocrystalline fcc NaCl-type structure with a mean crystallite size of 30 nm for the process #1 and only 3 nm for the process #5 [22,23]. Representative XRD patterns of CrC_xO_y samples prepared by DLICVD (process #5) in the temperature range 350-450 °C are shown in Fig. 3.

The CrN_xO_y coatings grown either by MOCVD with the gas mixture $Cr(CO)_6/N_2/NH_3$ or DLICVD using toluene as solvent exhibit a metallic lusture and yellowish gray color. They have a fine-grained surface morphology constituted of small grains with a 100 nm mean size and a compact structure (Fig. 4). Their crystallographic structure is comparable with that of CrC_xO_y and is strongly related to fcc CrN. Evidence for the nanostructure of these coatings is given by the mean crystallite size of 30 nm and 7 nm determined by XRD for the coatings grown by the processes #3 and #6, respectively.

3.3. Composition

Typical film composition is given in Table 2. Under N_2 ambient (process #1), the composition is close to the Cr_2CO ternary phase previously reported [23]. Addition of H_2 removes the C and the composition is $Cr_{0.39}O_{0.59}C_{0.02}$ that is close to the Cr_2O_3 stoichiometry. By DLICVD using THF the film composition is typically $Cr_{0.43}O_{0.40}C_{0.17}$. When toluene is used as solvent (process #5), an original oxide is obtained at 350 °C with Cr:O = 1:1 while the carbon content increases to 25% at higher temperature. The composition of the chromium oxynitrides coatings is more sensitive to the growth conditions. CrN can be deposited at 285 °C by MOCVD (process #3) while by changing the temperature and the mole fraction a significant amount of oxygen originating

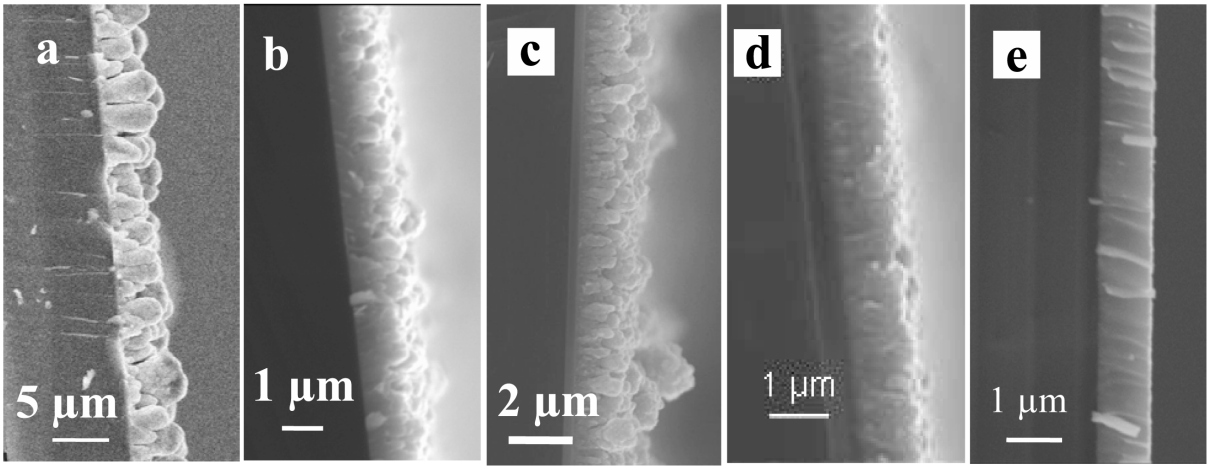

Fig. 2. Cross section SEM micrographs of CrCO coatings grown on Si by various processes: MOCVD #1 (a), MOCVD #2 (b), DLICVD #4 (c), DLICVD #5 at 350 °C (d), and 450 °C (e).

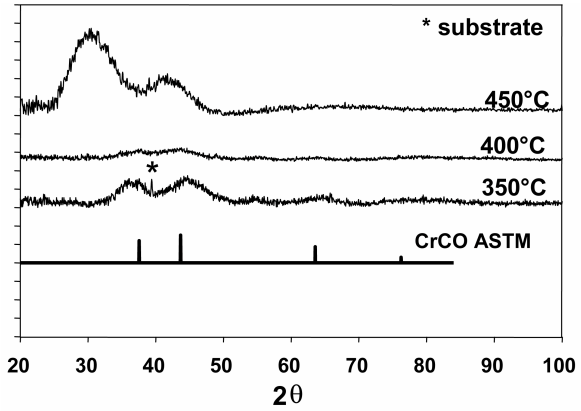

Fig. 3. XRD patterns of CrC_xO_y coatings grown by DLICVD (process #5) at different deposition temperature compared to the XRD pattern of CrCO from the literature.

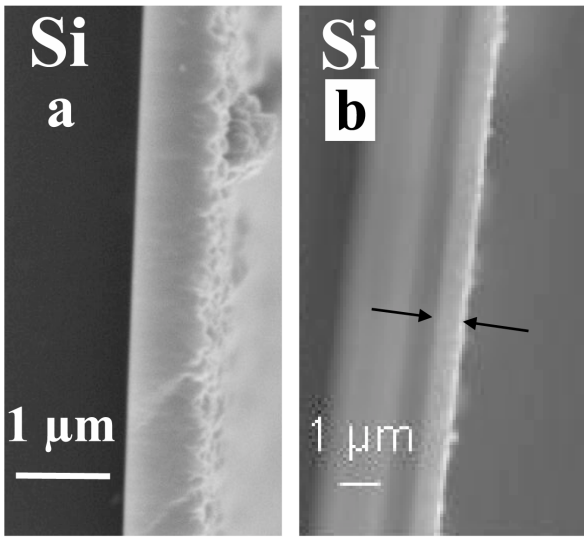

Fig. 4. Cross section SEM micrographs of CrNO (a) and CrNOC (b) coatings grown on Si by MOCVD #3 and DLICVD #6, respectively.

from the CO ligands is incorporated in the films. In this MOCVD #3 only traces of C were found. This is not the case by DLICVD (#6) where the solvent contributes to the C incorporation in the layers to form $Cr_{0.24}N_{0.26}O_{0.36}C_{0.13}$.

3.4. Thermal stability

By annealing under vacuum, the fcc nanocrystalline CrC_xO_y coatings undergo a transformation at 650 °C to form Cr_2O_3 and Cr_3C_2. This phase mixture is not surprising because they are in thermodynamic equilibrium at high temperature. When the C content is lower than the Cr_2CO stoichiometry, the coatings exhibit a lower thermal stability and the formation of Cr_2O_3 starts at 500 °C. After annealing at 500 °C for 5 h, the oxide $Cr_{0.39}O_{0.59}C_{0.02}$ formed under H_2 partial pressure (process #2) crystallizes with an fcc structure rather than that of Cr_2O_3 as expected because of the composition. Chromium oxides with fcc structure have already been reported but they had a Cr:O = 1:1 stoichiometry [24]. At higher temperature, further structural changes were observed. The CrN_xO_y coatings exhibit a high thermal stability since no change was observed in the XRD data after annealing at 650 °C for 5 h.

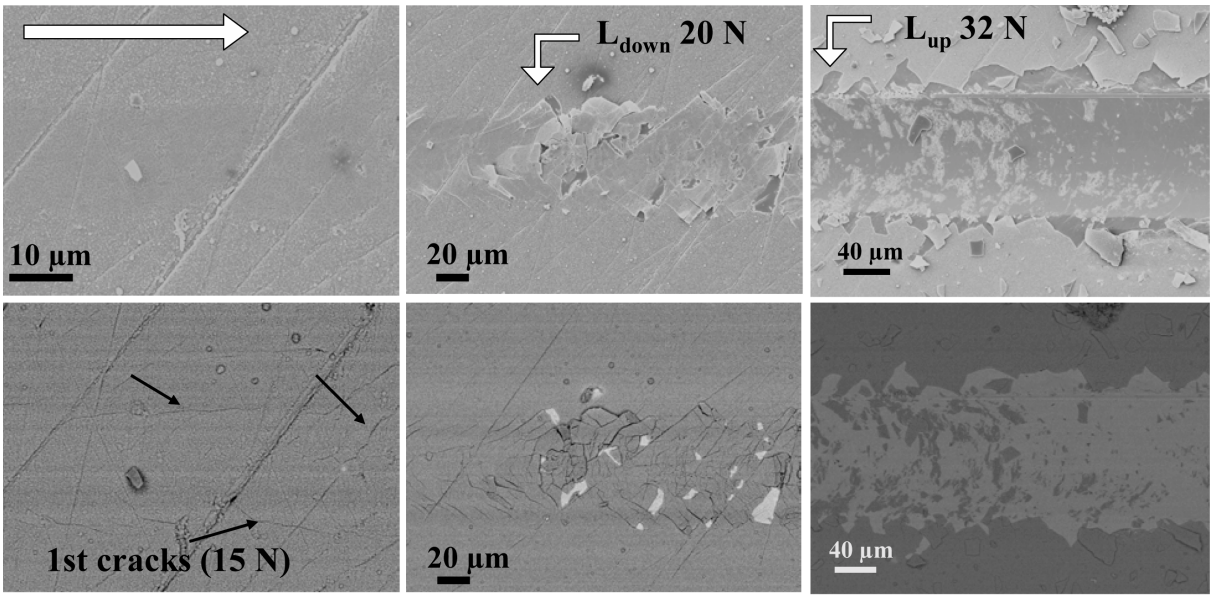

Fig. 5. SEM (top) and back scattered electron (bottom) images of a typical scratch track produced on a CrNO coating grown on stainless steel by MOCVD #3 (thickness 850 nm).

3.5. Mechanical properties

Hardness values are reported in Table 2. Unreliable hardness data for CrC_xO_y coatings deposited by the processes #1, 2 and 4 were discarded because of the high porosity and roughness of these samples (Fig. 2). As deposited CrC_xO_y DLICVD films grown using toluene have a high hardness of 16 GPa and an elastic modulus of 240 GPa. Change in the C content of these CrC_xO_y coatings does not affect significantly their hardness. This high hardness is comparable with that of MOCVD chromium carbides films [5,11]. Despite a compact morphology, a smooth surface (Fig. 4) and an fcc CrN-type structure, the CrN_xO_y coatings grown by MOCVD (#3) and DLICVD (#6) do not exhibit a high hardness (6 GPa). Certainly oxygen incorporation plays a major role since CrN is well known as hard coating.

Adhesion was investigated by scratch test. For CrC_xO_y grown by the process #1, a partial detachment of the coating started both inside and outside the scratch trace for a critical load L_{down} = 4-7 N. A continuous ductile perforation of the coating and a complete removal was observed for a critical load L_{up} = 35 N for a 4 µm thick coating and 22 N for a 2 mm thick coating. For oxide films made by the process #2 interfacial spallation was observed at the edge and the bottom of the scratch track for L_{down} = 9 N and the coating was completely removed from the track for L_{up} = 24 N. No significant difference was found for coatings with similar thickness grown by the processes #1, 2 and 4. These buckling and spallation failure modes are characteristic of a poor adhesion (adhesive-cohesive failure mode) [25]. This is in agreement with the porous structure of these coatings (Fig. 2).

The compact films CrC_xO_y (#5) and CrN_xO_y (#3) exhibit the same failure mode, which is significantly different than the one observed for the porous films. Typically, chevron shape cracks were first formed in the track, followed by interfacial spallation at the edge and the bottom of the scratch path (L_{down} determined by acoustic emission) and complete delaminating in the track above L_{up} (Fig. 5). Thus, for coatings with comparable thickness, chevron cracks were found around 2 N for CrC_xO_y (#5) and 15 N for CrN_xO_y (#3) while L_{down} was respectively, 5 and 20 N, and L_{up} was 25 and 35 N. This reveals a better adhesion of CrN_xO_y. The chevron cracks probably originate from tensile stresses behind the moving stylus. They do not propagate out of the track indicating that a sufficient stress relief occurs. This is characteristic of a brittle failure mode as observed frequently for ceramic coatings. This co-

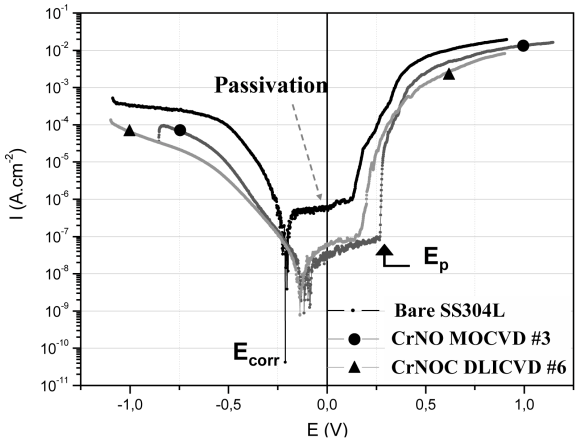

Fig. 6. Polarization curves obtained in aerated NaCl 0.5M solution for two coatings deposited on stainless steel: CrNO MOCVD #3 (thickness 500 nm) and CrNOC DLICVD #6 (700 nm) compared to the bare SS304L substrate.

hesive failure is characteristic of good adhesion properties [25].

3.6. Corrosion tests

Both polarization curves and electrochemical impedance spectroscopy (EIS) were used for the corrosion tests in aerated and neutral NaCl solution (0.5 M) which generates localized pitting corrosion of stainless steel. The first method provides rapid information on the corrosion behavior while the second is used to assess the protective properties of the coatings. Typical polarization curves are plotted in Fig. 6. As expected, stainless steel chosen as reference shows the corrosion potential (E_{cor}), a passivity plateau and the pitting potential (E_p). For a good protective coating in this solution it is expected a broader passivity plateau with a significant lowering of the current density but, for this test, defects in the coating play a major role. Samples prepared by the processes #1 and 4 were not tested because of their high porosity. Similarly, a passivity breakdown was found for an oxygen rich CrC_xO_y film grown by MOCVD #2 due to its porosity (Fig. 2). The CrNO (#3) and CrNOC (#6) coatings are more compact and they show generally a decrease of the cathodic current and an increase of E_{cor} and E_p. This is consistent with an efficient passivation of the surface compared to SS304L. From the data determined from the polarization curves coupled with observations of the samples after the test, the coatings can be ranked according to their protective properties against corrosion in neutral NaCl solution as CrNO #3 > CrNOC #6 > CrO #2. The EIS data confirm that chromium oxynitrides improve the corrosion resistance of SS304L. Indeed the polarization resistance R_p is higher for the coated samples compared to SS304L. The R_p values of CrNO films (process #3) are higher than that of CrNOC (#6) while there is no significant difference between CrO (#2) and bare SS304L, which is in good agreement with the above rating. Furthermore, for CrNO films, R_p increases with the thickness indicating an increase of the corrosion resistance.

4. CONCLUSIONS

CrC_xO_y coatings were grown using $Cr(CO)_6$ under atmospheric pressure in various ambient of different CVD processes: N_2 (#1) and H_2 (#2) for MOCVD and THF (#4) and toluene (#5) for DLICVD. Depending on the conditions, their composition varies typically from Cr_2CO to CrO where oxygen originates essentially from the dissociative adsorption of CO ligands. These CrC_xO_y films exhibit an fcc nanocrystalline structure. They are thermally stable up to 500 °C but, except those obtained from process #5, their cauliflower-like morphology is unsuitable for mechanical and protective properties. The CrC_xO_y films grown by DLICVD using toluene (#5) are significantly different. Their feature is attractive for hard metallurgical coatings with a good compactness, a high hardness (16 GPa) and a good adherence on SS304L. At this stage, the main limitation of DLICVD process using toluene as solvent for the growth of CrC_xO_y coatings is a relatively low growth rate compared to MOCVD but no attempt was made to optimize it in this preliminary work.

Addition of NH_3 in MOCVD (#3) and DLICVD (#6) allows the growth of CrN_xO_y and $CrN_xO_yC_z$ films, respectively. The composition can be changed from CrN to CrN_xO_y by MOCVD and carbon incorporation occurs by DLICVD originating from the solvent but all these coatings exhibit a very compact morphology and the fcc CrN-type structure. They are thermally stable for $T > 650$ °C but they have a low hardness. Adhesion on SS304L is very good and they could be used as protective coatings against corrosion. Further works are in progress especially to optimize the growth rate.

ACKNOWLEDGEMENTS

F. Frade Suarez and M. Nadal are gratefully acknowledged for their assistance.

References

[1] R. Hiskes, S.A. DiCarolis, J.L. Young, S.S. Laderman, R.D. Jacowitz and R.C. Taber // *Appl. Phys. Lett.* **59** (1991) 606.
[2] D.A. Edwards, R.M. Harker, M.F. Mahon and K.C. Molloy // *J. Mat. Chem.* **9** (1999) 1771.
[3] A.R. Kaul and B. V. Seleznev // *J. Physique IV* **3** (1993) 375.
[4] F. Felten, J.P. Sénateur, F. Weiss, R. Madar and A. Abrutis // *J. Phys. IV* **C5** (1995) 1079.
[5] F. Maury, F. Ossola and F. Senocq // *Surf. Coat. Technol.* **133-134** (2000) 198.
[6] A. Abrutis, J.P. Sénateur, F. Weiss, V. Kubilius, V. Bigelytč, Z. Saltylč, B. Vengalis and A. Jukna // *Supercond. Sci. Technol.* **10** (1997) 959.
[7] J.P. Endle, Y.M. Sun, N. Nguyen, S. Madhukar, R.L. Hance, J.M. White and J.G. Ekerdt // *Thin Solid Films* **388** (2001) 126.
[8] L. Gao, P. Härter, Ch. Linsmeier, J. Gstöttner, R. Emling and N. Schmitt-Landsiedel // *Mat. Sci. Semicond. Processing* **7** (2004) 331.
[9] J.P. Endle, Y.M. Sun, J. Silverman, N. Nguyen, A.H. Cowley, J.M. White and J.G. Ekerdt // *Thin Solid Films* **385** (2001) 66.
[10] F. Maury // *Electrochimica Acta* **50** (2005) 4525.
[11] F. Schuster, F. Maury, J.F. Nowak and C. Bernard // *Surf. Coat. Technol.* **46** (1991) 275.
[12] F. Schuster, F. Maury and J. F. Nowak // *Surf. Coat, Technol.* **43-44** (1990) 185.
[13] A. Douard and F. Maury // *Surf. Coat. Technol.* **200** (2005) 1407.
[14] A. Douard and F. Maury // *Surf. Coat. Technol.* **200** (2006) 6267.
[15] H. Lux and A. Ignatowicz // *Chem. Berich.* **101** (1968) 809.
[16] T. Kado and Y.J. Noda // *Jap. J. Appl. Phys.* **28** (1989) 1450.
[17] M. Kmetz, B.J. Tan, W. Willis and S. Suib // *J. Mat. Sci.* **26** (1991) 2107.
[18] T. Kado // *J. Am. Ceram. Soc* **82** (1999) 3245.
[19] T. Kado and Q. Fan // *J. Am. Ceram. Soc* **84** (2001) 1763.
[20] S. Agouram, F. Bodart and G. Terwagne // *Surf. Coat. Technol.* **180-181** (2004) 164.
[21] W.C. Oliver and G.M. Pharr // *J. Mat. Res.* **7** (1992) 1564.
[22] M. Kmetz, B.J. Tan, W. Willis and S. Suib // *J. Mat. Sci.* **26** (1991) 2107.
[23] I.M. Watson and J.A. Connor // *Polyhedron* **8** (1989) 1794.
[24] V. Dufek, F. Petru and V. Brozek // *Monatsch. Chem.* **98** (1967) 2424.
[25] P.J. Burnett and D.S. Rickerby // *Thin Solid Films* **154** (1987) 403.